Progress In Electromagnetics Research B, Vol. 33, 317–337, 2011

THE E-PILE+SMCG FOR SCATTERING FROM AN OBJECT BELOW 2D SOIL ROUGH SURFACE

W.-J. Ji * **and C.-M. Tong**

Missile Institute, Air Force Engineering University, P. O. Box 25, Sanyuan, Shannxi 713800, China

Abstract—A rigorous fast numerical method called E-PILE+SMCG is introduced and then used in a Monte Carlo study of scattering from a three dimensional perfectly electrical conductor (PEC) object below lossy soil rough surface. This method is the three dimensional (3D) extendability of PILE (Propagation-Inside-Layer Expansion) method which is proposed for two dimensional (2D) scattering problem. The rough surface with Gaussian profile is used to emulate the realistic situation of statistically rough surface, while the tapered incident wave is chosen to reduce the truncation error. The 3D angular correlation function (ACF) and bistatic scattering coefficient (BSC) are studied and applied to the detection of a target embedded in the clutter. The ACF is computed by using numerical method with circular azimuthal angle averaging technique. Because of its success in suppressing the clutter scattering, the technique appears attractive in real life implementation.

1. INTRODUCTION

Electromagnetic sensing of buried objects in the presence of random rough surface is important due to applications in the detection of subsurface pipes, landmines, etc. Some approximate analytical models have been derived in the small roughness limit problem [1, 2]. However, the complexity of the problem has limited the development of more general approximations. Some works have explored numerical solutions [3–5], but have concentrated primarily on two dimensional scattering problems to reduce computational complexity. The two dimensional rough surface ground (i.e., three dimensional (3D) scattering problem) is a more realistic problem as investigated by

Received 10 June 2011, Accepted 8 August 2011, Scheduled 12 August 2011

* Corresponding author: Wei-Jie Ji (jiweijie01@163.com).

mangy researchers [6–8]. In [8], the EM scattering from a 3D shallow object buried under a 2D random rough dielectric surface is analyzed by using the steepest descent fast multi-pole method. However, the random surface and object are modeled as a whole, which make it difficult to apply this method treating larger and complex problems.

In the numerical simulations of the scattering by an object under a rough surface, the size of the surface plays an important role: the unknown number of surface is much lager than that of the object. So it is interesting to investigate exact fast numerical methods to treat this large problem. For instance, the sparse matrix/canonical grid algorithm (SMCG) of Tsang et al. with the complexity of $O(N \log N)$ in [9–11], the novel acceleration forward backward method (FB/NSA) of Torrungrueng et al. with the complexity of $(O(N))$ in [12], the steepest descent fast multi-pole method (SDFMM) of Jandhyala et al. with the complexity of $(O(N))$ in [13]. In [14], the general sparse matrix/canonical grid algorithm (G-SMCG) is introduced to compute the electromagnetic scattering from object on ocean surface. For the problem of an object under a rough surface, the interaction between rough surface and object must be considered. These methods cannot be applied since there are two different and distinct surfaces.

Recently, Dechamps et al. developed a fast numerical method, PILE (Propagation-Inside-Layer Expansion) [15], devoted to the scattering by a stack of two one dimensional (1D) interfaces separating homogeneous media. Bourlier et al. have applied the PILE method for an object located below a 1D rough surface [16]. The main advantage of the PILE method is that the resolution of the linear system (obtained from the method of moments) is broken up into different steps: Two steps are dedicated to solving for the local interactions, which can be done from efficient methods valid for a single rough surface, such as SMCG and FB/NSA. Two steps are dedicated to solving for the coupling interactions. The purpose of this paper is to extend the PILE method to the 3D scattering problem of an object buried under soil rough surface. In order to accelerate the extended PILE method and to treat a large problem, the local interactions of the rough surface are computed by using SMCG because of its relative simplicity of programming and low complexity of computation.

To characterize object below the rough surface, the angular correlation function (ACF) and bistatic scattering coefficient (BSC) are utilized. The ACF is the correlation function of two scattering fields in two different directions, corresponding to two incident fields. In [17–20], the ACF of rough surface is studied by analytical and numerical methods, and the results are compared with experimental. The ACF has also been applied to the detection of a buried object [21, 22]. For

the detection of a object under a rough surface, the scattering of the object is often obscured by clutter such as rough surface scattering and random medium scattering, which makes it difficult to detection the object. From [21, 22], we known that by making use of the ACF, the contribution of clutter to the angular correlation function is minimal away from the memory line, making the contribution of the buried object more conspicuous by many dB. In this paper, we study the ACF of wave scattering by an object buried under soil rough surface for 3D scattering problems. For the ACF applied in detecting buried object, the object is associated with one realization of the random rough surface, therefore realization averaging is meaningless. In the 3D ACF, we make the circular azimuthal angle averaging, which is successful for detection the 3D object.

2. THEORY AND FORMULATION

Figure 1 illustrates the basic geometry considered in this paper: a PEC object is located below a rough surface. The rough interface between free space and a dielectric medium with relative complex permittivity ε_1 is described by $z = f(x, y)$, and generated by Monte Karlo method. The θ_i and φ_i are incident angles, and the θ_s and φ_s are scattering angles.

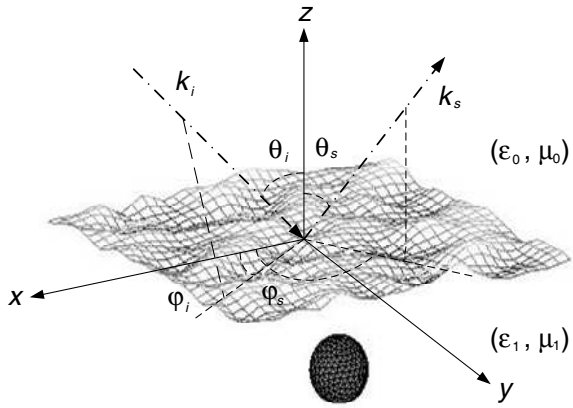

Figure 1. The geometry of a PEC object buried under rough surface.

2.1. The Boundary Integral Equations

To avoid edge limitations, the incident field is tapered so that the illuminated rough surface can be confined to the surface area $L_x \times L_y$. Consider the tapered plane wave incident on the structure along

$\hat{\mathbf{k}}_i = \sin\theta_i\cos\varphi_i\hat{\mathbf{x}} + \sin\theta_i\sin\varphi_i\hat{\mathbf{y}} - \cos\theta_i\hat{\mathbf{z}}$. Then the incident fields can be expressed in terms of spectrum of the incident wave [9, 270–368]

$$\begin{aligned}\mathbf{H}^{inc}(x,y,z) &= -\frac{1}{\eta}\int_{-\infty}^{\infty}dk_x\int_{-\infty}^{\infty}dk_y\exp(ik_xx+ik_yy-ik_zz)\\ &\quad\cdot E_{TE}(k_x,k_y)\hat{\mathbf{h}}(-k_z) \qquad (1)\\ \mathbf{E}^{inc}(x,y,z) &= \int_{-\infty}^{\infty}dk_x\int_{-\infty}^{\infty}dk_y\exp(ik_xx+ik_yy-ik_zz)\\ &\quad\cdot E_{TE}(k_x,k_y)\hat{\mathbf{e}}(-k_z) \qquad (2)\end{aligned}$$

where $E_{TE}(k_x,k_y)$ represents the spectrum of the incident field, defined as

$$\begin{aligned}E_{TE}(k_x,k_y) &= \frac{1}{4\pi^2}\int_{-\infty}^{\infty}dx\int_{-\infty}^{\infty}dy\exp(-ik_xx-ik_yy)\\ &\quad\cdot\exp(i(k_{ix}x+k_{iy}y)(1+w))\exp(-t) \qquad (3)\\ t &= t_x+t_y=\left(x^2+y^2\right)/g^2 \qquad (4)\\ t_x &= \frac{(\cos\theta_i\cos\varphi_ix+\cos\theta_i\sin\varphi_iy)^2}{g^2\cos^2\theta_i} \qquad (5)\\ t_y &= \frac{(-\sin\varphi_ix+\cos\varphi_iy)^2}{g^2} \qquad (6)\\ w &= \frac{1}{k_0^2}\left[\frac{(2t_x-1)}{g^2\cos^2\theta_i}+\frac{(2t_y-1)}{g^2}\right] \qquad (7)\end{aligned}$$

The parameter g controls the tapering of the incident wave. In the above, k_0 and η are the wave-number and wave impedance of free space respectively, and $\hat{\mathbf{e}}$, $\hat{\mathbf{h}}$ denote the polarization vectors.

For TE wave incidence

$$\begin{aligned}\hat{\mathbf{e}}(-k_z) &= \frac{1}{k_\rho}(\hat{\mathbf{x}}k_y-\hat{\mathbf{y}}k_x) \qquad (8)\\ \hat{\mathbf{h}}(-k_z) &= \frac{k_z}{k_0k_\rho}(\hat{\mathbf{x}}k_x-\hat{\mathbf{y}}k_y)+\frac{k_\rho}{k_0}\hat{\mathbf{z}} \qquad (9)\end{aligned}$$

And for TM wave incidence

$$\begin{aligned}\hat{\mathbf{h}}(-k_z) &= -\frac{1}{k_\rho}(\hat{\mathbf{x}}k_y-\hat{\mathbf{y}}k_x) \qquad (10)\\ \hat{\mathbf{e}}(-k_z) &= \frac{k_z}{k_0k_\rho}(\hat{\mathbf{x}}k_x-\hat{\mathbf{y}}k_y)+\frac{k_\rho}{k_0}\hat{\mathbf{z}} \qquad (11)\end{aligned}$$

with $k_z=\sqrt{k_0^2-k_\rho^2}$ and $k_\rho=\sqrt{k_x^2+k_y^2}$.

Let $\mathbf{r}' = x'\hat{\mathbf{x}} + y'\hat{\mathbf{y}} + f(x', y')\hat{\mathbf{z}}$ and $\mathbf{r} = x\hat{\mathbf{x}} + y\hat{\mathbf{y}} + f(x, y)\hat{\mathbf{z}}$ denote source point and field point separately. The fields in region 0 and region 1 satisfy the following equations [9, 552–576]:

$$\begin{aligned}
&\frac{\mathbf{J}_r(\mathbf{r})}{2} - \hat{\mathbf{n}} \times \left\{ \int_S (-i\omega)\mathbf{M}_r(\mathbf{r}')\varepsilon_0 G_0 ds' \right. \\
&\left. + P\int_S [(\mathbf{J}_r(\mathbf{r}')) \times \nabla' G_0 + \hat{\mathbf{n}} \cdot \mathbf{H}_r(\mathbf{r}')\nabla' G_0] ds' \right\} \\
&= \hat{\mathbf{n}} \times (\mathbf{H}^{inc}(\mathbf{r}) + \mathbf{H}_o^{sac}(\mathbf{r})) \quad (\mathbf{r} \in S) \qquad (12) \\
&\frac{\hat{\mathbf{n}} \cdot \mathbf{E}_r(\mathbf{r})}{2} - \hat{\mathbf{n}} \cdot \left\{ \int_S \mathbf{J}_r(\mathbf{r}') i\omega\mu G_0 ds' \right. \\
&\left. + P\int_S [\mathbf{M}_r(\mathbf{r}') \times \nabla' G_0 + \hat{\mathbf{n}} \cdot \mathbf{E}_r(\mathbf{r}')\nabla' G_0] ds' \right\} \\
&= \hat{\mathbf{n}} \cdot (\mathbf{E}^{inc}(\mathbf{r}) + \mathbf{E}_o^{sac}(\mathbf{r})) \quad (\mathbf{r} \in S) \qquad (13) \\
&-\frac{\mathbf{M}_r(\mathbf{r})}{2} - \hat{\mathbf{n}} \times \left\{ \int_S \mathbf{J}_r(\mathbf{r}') i\omega\mu G_1 ds' \right. \\
&\left. + P\int_S [(\mathbf{M}_r(\mathbf{r}')) \times \nabla' G_1 + \hat{\mathbf{n}} \cdot \mathbf{E}_r(\mathbf{r}')\nabla' G_1] ds' \right\} \\
&= -\hat{\mathbf{n}} \times \mathbf{E}_o^{sac}(\mathbf{r}) \quad (\mathbf{r} \in S) \qquad (14) \\
&-\frac{\hat{\mathbf{n}} \cdot \mathbf{H}_r(\mathbf{r})}{2} - \hat{\mathbf{n}} \cdot \left\{ \int_S (-i\omega)\mathbf{M}_r(\mathbf{r}')\varepsilon_1 G_1 ds' \right. \\
&\left. + P\int_S [(\mathbf{J}_r(\mathbf{r}')) \times \nabla' G_1 + \hat{\mathbf{n}}' \cdot \mathbf{H}_r(\mathbf{r}')\nabla' G_1] ds' \right\} \\
&= -\hat{\mathbf{n}} \cdot \mathbf{H}_o^{sac}(\mathbf{r}) \quad (\mathbf{r} \in S) \qquad (15)
\end{aligned}$$

$$\mathbf{E}_r^{sac}(\mathbf{r})|_{\tan} = i\omega\mu_1 \int_{S_b} \left[\mathbf{J}_o(\mathbf{r}') + \frac{1}{k_q^2} \nabla(\nabla' \cdot (\mathbf{J}_o(\mathbf{r}'))) \right] G_1 ds' \ (\mathbf{r} \in S_b) \qquad (16)$$

where, $G_{0,1} = \frac{\exp(ik_{0,1}R)}{4\pi R}$ and $R = \sqrt{(x-x')^2 + (y-y')^2 + (f(x,y) - f(x',y'))^2}$, k_0 and k_1 are the wave-number of the upper and lower medium, S denotes the rough surface, and S_b denotes the surface of object. $\mathbf{J}_o(\mathbf{r}) = \hat{\mathbf{n}}_o \times \mathbf{H}_o(\mathbf{r})$, $\mathbf{M}_r(\mathbf{r}) = \hat{\mathbf{n}} \times \mathbf{E}_r(\mathbf{r})$, $\mathbf{J}_r(\mathbf{r}) = \hat{\mathbf{n}} \times \mathbf{H}_r(\mathbf{r})$. The unit normal vector $\hat{\mathbf{n}}$ and $\hat{\mathbf{n}}'$ refer to primed coordinates and point away from the lower medium, $\hat{\mathbf{n}}_o$ and $\hat{\mathbf{n}}_o'$ point away from the object.

$$\mathbf{H}_o^{sac}(\mathbf{r}) = \int_{S_b} \mathbf{J}_o(\mathbf{r}') \times \nabla' G_1 ds' \qquad (17)$$

$$\mathbf{E}_o^{sac}(\mathbf{r}) = -\frac{i}{\omega\varepsilon_1} \nabla \times \int_{S_b} \mathbf{J}_o(\mathbf{r}') \times \nabla' G_1(\mathbf{r}, \mathbf{r}') ds' \qquad (18)$$

$$\mathbf{E}_r^{sac}(\mathbf{r}) = -\int_S [(-i\omega\mu_1)\mathbf{J}_r(\mathbf{r}')G_1 + \mathbf{M}_r(\mathbf{r}') \times \nabla' G_1 + \nabla' G_1 \hat{\mathbf{n}}' \cdot \mathbf{E}_r(\mathbf{r}')]ds' \tag{19}$$

The $\mathbf{H}_o^{sac}$ and $\mathbf{E}_o^{sac}$ denote the scattering field from object to rough surface, and $\mathbf{E}_r^{sac}$ denote the scattering field from upper surface to object.

2.2. The E-PILE Method

The integral equations of rough surface is discretized by using Method of Moment (MoM) with pulse base function. Therefore, the integral equations of object is discretized by using MoM with the Rao-Wilton-Glisson (RWG) base function which is introduced in [23]. After discretizing Equations (12)–(19), we get the following matrix equation

$$\mathbf{ZX} = \mathbf{V} \tag{20}$$

where $\mathbf{Z}$ is the total impedance matrix of size $(N + M) \times (N + M)$ (N is the number of unknown belongs to rough surface, and M is the number of unknown belongs to object). $\mathbf{V}$ is the incidence field vector.

$$\mathbf{V}^T = \left[\mathbf{V}_r^T \mathbf{V}_o^T\right] \tag{21}$$

$\mathbf{V}_r^T$ is the incidence field vector of rough surface. For 2D dielectric rough surface

$$\mathbf{V}_r^T = [\mathbf{F}_x^{inc}, \mathbf{F}_y^{inc}, 0, 0, 0, \mathbf{J}_n^{inc}] \tag{22}$$

with

$$F_x^{inc}(\mathbf{r}) = \sqrt{1 + \left(\frac{\partial f(x,y)}{\partial x}\right)^2 + \left(\frac{\partial f(x,y)}{\partial y}\right)^2}\, \hat{\mathbf{n}} \times \mathbf{H}_r^{inc}(\mathbf{r}) \cdot \hat{\mathbf{x}} \tag{23a}$$

$$F_y^{inc}(\mathbf{r}) = \sqrt{1 + \left(\frac{\partial f(x,y)}{\partial x}\right)^2 + \left(\frac{\partial f(x,y)}{\partial y}\right)^2}\, \hat{\mathbf{n}} \times \mathbf{H}_r^{inc}(\mathbf{r}) \cdot \hat{\mathbf{y}} \tag{23b}$$

$$J_n^{inc}(\mathbf{r}) = \sqrt{1 + \left(\frac{\partial f(x,y)}{\partial x}\right)^2 + \left(\frac{\partial f(x,y)}{\partial y}\right)^2}\, \hat{\mathbf{n}} \cdot \mathbf{E}_r^{inc}(\mathbf{r}) \tag{23c}$$

$\mathbf{V}_o^T$ is the incidence field vector of object. Because the object is buried under the rough surface, so we have $\mathbf{V}_o^T = 0$.

$\mathbf{X}$ is the unknown vector.

$$\mathbf{X}^T = [\mathbf{X}_r^T \mathbf{X}_o^T] \tag{24}$$

$\mathbf{X}_r^T$ is the unknown vector of rough surface, and the unknowns are the six field components on the rough surface.

$$\mathbf{X}_r^T = [\mathbf{F}_x^T, \mathbf{F}_y^T, \mathbf{F}_n^T, \mathbf{J}_x^T, \mathbf{J}_y^T, \mathbf{J}_n^T] \tag{25}$$

with

$$F_x(\mathbf{r}) = \sqrt{1+\left(\frac{\partial f(x,y)}{\partial x}\right)^2+\left(\frac{\partial f(x,y)}{\partial y}\right)^2}\,\hat{\mathbf{n}}\times\mathbf{H}_r(\mathbf{r})\cdot\hat{\mathbf{x}} \quad (26a)$$

$$F_y(\mathbf{r}) = \sqrt{1+\left(\frac{\partial f(x,y)}{\partial x}\right)^2+\left(\frac{\partial f(x,y)}{\partial y}\right)^2}\,\hat{\mathbf{n}}\times\mathbf{H}_r(\mathbf{r})\cdot\hat{\mathbf{y}} \quad (26b)$$

$$F_n(\mathbf{r}) = \sqrt{1+\left(\frac{\partial f(x,y)}{\partial x}\right)^2+\left(\frac{\partial f(x,y)}{\partial y}\right)^2}\,\hat{\mathbf{n}}\cdot\mathbf{H}_r(\mathbf{r}) \quad (26c)$$

$$J_x(\mathbf{r}) = \sqrt{1+\left(\frac{\partial f(x,y)}{\partial x}\right)^2+\left(\frac{\partial f(x,y)}{\partial y}\right)^2}\,\hat{\mathbf{n}}\times\mathbf{E}_r(\mathbf{r})\cdot\hat{\mathbf{x}} \quad (26d)$$

$$J_y(\mathbf{r}) = \sqrt{1+\left(\frac{\partial f(x,y)}{\partial x}\right)^2+\left(\frac{\partial f(x,y)}{\partial y}\right)^2}\,\hat{\mathbf{n}}\times\mathbf{E}_r(\mathbf{r})\cdot\hat{\mathbf{y}} \quad (26e)$$

$$J_n(\mathbf{r}) = \sqrt{1+\left(\frac{\partial f(x,y)}{\partial x}\right)^2+\left(\frac{\partial f(x,y)}{\partial y}\right)^2}\,\hat{\mathbf{n}}\cdot\mathbf{E}_r(\mathbf{r}) \quad (26f)$$

$\mathbf{X}_o^T$ is the unknown vector of object, and the unknown is the surface current on the object.

$$\mathbf{X}_o^T = [\mathbf{J}_{o1}, \mathbf{J}_{o2}, \mathbf{J}_{o3}] \quad (27)$$

with

$$J_{o1}(\mathbf{r}) = \hat{\mathbf{n}}\times\mathbf{H}_o(\mathbf{r})\cdot\hat{\mathbf{x}} \quad (28a)$$

$$J_{o2}(\mathbf{r}) = \hat{\mathbf{n}}\times\mathbf{H}_o(\mathbf{r})\cdot\hat{\mathbf{y}} \quad (28b)$$

$$J_{o3}(\mathbf{r}) = \hat{\mathbf{n}}\times\mathbf{H}_o(\mathbf{r})\cdot\hat{\mathbf{z}} \quad (28c)$$

In order to solve efficiency the linear system (20), the impedance matrix is expressed from sub-matrices as [14]

$$\mathbf{Z} = \begin{bmatrix} \mathbf{Z}^r & \mathbf{Z}^{o\to r} \\ \mathbf{Z}^{r\to o} & \mathbf{Z}^o \end{bmatrix} \quad (29)$$

$\mathbf{Z}^r$ and $\mathbf{Z}^o$ correspond exactly to the self-impedance matrices of rough surface and object.

$$\mathbf{Z}^r = \begin{bmatrix} \langle p_m, \mathbf{H}_r^{sac}(\mathbf{r}, p_n)\rangle \\ \langle p_m, \mathbf{E}_r^{sac}(\mathbf{r}, p_n)\rangle \end{bmatrix} \quad (\mathbf{r}\in S) \quad (30)$$

where, $\langle,\rangle$ denotes surface integration. p_m and p_n is the pulse basis.

$$\mathbf{Z}^o = \left[\langle f_m, \mathbf{E}_o^{sac}(\mathbf{r}, j_n)\rangle_{S_b}\right] \quad (\mathbf{r}\in S_b) \quad (31)$$

A popular choice for the functions j_n and f_m is the RWG basis, which will be used here.

The matrices $\mathbf{Z}^{o\to r}$ and $\mathbf{Z}^{r\to o}$ can be interpreted as coupling impedance matrices between object and upper surface.

$$\mathbf{Z}^{o\to r} = \begin{bmatrix} \langle f_m, \mathbf{H}_o^{sac}(\mathbf{r}, f_n)\rangle \\ \langle f_m, \mathbf{E}_o^{sac}(\mathbf{r}, f_n)\rangle \end{bmatrix} \quad (\mathbf{r} \in S) \tag{32}$$

$$\mathbf{Z}^{r\to o} = [\langle p_m, \mathbf{E}_r^{sac}(r, p_n)\rangle] \quad (\mathbf{r} \in S_b) \tag{33}$$

The reverse of the matrix $\mathbf{Z}$ is:

$$\mathbf{Z}^{-1} = \begin{bmatrix} \mathbf{T} & \mathbf{U} \\ \mathbf{Q} & \mathbf{W} \end{bmatrix} \tag{34}$$

where

$$\mathbf{T} = (\mathbf{Z}^r - \mathbf{Z}^{o\to r}(\mathbf{Z}^o)^{-1}\mathbf{Z}^{r\to o})^{-1} \tag{35a}$$

$$\mathbf{U} = -(\mathbf{Z}^r - \mathbf{Z}^{o\to r}(\mathbf{Z}^o)^{-1}\mathbf{Z}^{r\to o})^{-1}\mathbf{Z}^{o\to r}(\mathbf{Z}^o)^{-1} \tag{35b}$$

$$\mathbf{Q} = -(\mathbf{Z}^o)^{-1}\mathbf{Z}^{r\to o}(\mathbf{Z}^r - \mathbf{Z}^{o\to r}(\mathbf{Z}^o)^{-1}\mathbf{Z}^{r\to o})^{-1} \tag{35c}$$

$$\mathbf{W} = (\mathbf{Z}^o)^{-1} + (\mathbf{Z}^o)^{-1}\mathbf{Z}^{r\to o}(\mathbf{Z}^r - \mathbf{Z}^{o\to r}(\mathbf{Z}^o)^{-1}\mathbf{Z}^{r\to o})^{-1}\mathbf{Z}^{o\to r}(\mathbf{Z}^o)^{-1} \tag{35d}$$

By using Equations (34) and (35), the total field on the rough surface can be expressed as

$$\mathbf{X}_r = (\mathbf{Z}^r - \mathbf{Z}^{o\to r}(\mathbf{Z}^o)^{-1}\mathbf{Z}^{r\to o})^{-1}(\mathbf{V}_r - \mathbf{Z}^{o\to r}(\mathbf{Z}^o)^{-1}\mathbf{V}_o) \tag{36}$$

Because the object is buried under the rough surface, so $\mathbf{V}_o^T = 0$. Thus Equation (36) can be expressed as:

$$\begin{aligned} \mathbf{X}_r &= (\mathbf{Z}^r - \mathbf{Z}^{o\to r}(\mathbf{Z}^o)^{-1}\mathbf{Z}^{r\to o})^{-1}\mathbf{V}_r \\ &= (\mathbf{I} - (\mathbf{Z}^r)^{-1}\mathbf{Z}^{o\to r}(\mathbf{Z}^o)^{-1}\mathbf{Z}^{r\to o})^{-1}(\mathbf{Z}^r)^{-1}\mathbf{V}_r \end{aligned} \tag{37}$$

where $\mathbf{I}$ is the identity matrix. Let us introduce the characteristic matrix $\mathbf{M}_c$ as

$$\mathbf{M}_c = (\mathbf{Z}^r)^{-1}\mathbf{Z}^{o\to r}(\mathbf{Z}^o)^{-1}\mathbf{Z}^{r\to o} \tag{38}$$

Then the first term in Equation (37) can be expanded as an infinite series over p

$$(\mathbf{I} - (\mathbf{Z}^r)^{-1}\mathbf{Z}^{o\to r}(\mathbf{Z}^o)^{-1}\mathbf{Z}^{r\to o})^{-1} = \sum_{p=0}^{p=\infty} \mathbf{M}_c^p \tag{39}$$

For the numerical computation, the sum must be truncated at order P_{PILE}. Combing the Equations (38) and (39), the total unknown vector on the rough surface is then expressed as

$$\mathbf{X}_r = \left[\sum_{p=0}^{p=p_{\text{PILE}}} \mathbf{M}_c^p\right](\mathbf{Z}^r)^{-1}\mathbf{V}_r = \sum_{p=0}^{p=p_{\text{PILE}}} \mathbf{Y}_r^{(p)} \tag{40}$$

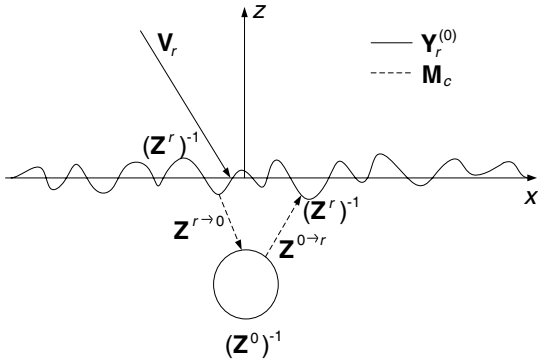

Figure 2. The physical interpretation of the $\mathbf{M}_c$.

We define the norm $\|\mathbf{M}_c\|$ of a complex matrix by its spectral radius, i.e., the modulus of its eigenvalue which has the highest modulus. Expansion (40) is accurate if $\|\mathbf{M}_c\|$ is inferior to 1. $\mathbf{Y}_r^{(p)}$ is defined as

$$\begin{cases} \mathbf{Y}_r^{(0)} = (\mathbf{Z}^r)^{-1}\mathbf{V}_r & \text{for} \quad p = 0 \\ \mathbf{Y}_r^{(p)} = \mathbf{M}_c\mathbf{Y}_r^{(p-1)} & \text{for} \quad p > 0 \end{cases} \tag{41}$$

The physical interpretation of $\mathbf{M}_c$ is shown in Figure 2: in the zeroth order term, $(\mathbf{Z}^r)^{-1}$ accounts for the local interactions on the upper rough surface, so $\mathbf{Y}_r^{(0)}$ corresponds to the contribution of the scattering on the rough surface when it is illuminated by the direct incident field $\mathbf{V}_r$. In the first order, $\mathbf{Z}^{r\to o}$ propagates the field on the rough surface toward the object, $(\mathbf{Z}^o)^{-1}$ corresponds to the contribution of the scattering on the object, and $\mathbf{Z}^{o\to r}$ propagates the field on the object toward the upper surface again. Finally, $(\mathbf{Z}^r)^{-1}$ updates the field values on the upper rough surface. So the characteristic $\mathbf{M}_c$ realizes a back and forth between the upper surface and the lower object. In a word, the order P_{PILE} of PILE corresponds to the back and forth interaction between the upper surface and object.

2.3. Acceleration of E-PILE by Using the SMCG

The advantage of the PILE method is that the most complex operations, which is $(\mathbf{Z}^r)^{-1}\mathbf{u}$ in (40) ($\mathbf{u}$ is a vector), only concern the local interactions on rough surface and can be calculated by fast numerical methods that already exist for single 2D rough surface, like for instance the SMCG. The SMCG will be used in this paper because of its relative simplicity of programming and low complexity

of computation. It is based on the fact that performing $(\mathbf{Z}^r)^{-1}\mathbf{u}$ is equivalent to solving $\mathbf{Z}^r\mathbf{v} = \mathbf{u}$ for $\mathbf{v}$, this latter problem can be solved iteratively by using a conjugate gradient scheme as Pre-BICGtab. At each iteration, it is necessary to compute $\mathbf{Z}^r\mathbf{v}$, where $\mathbf{v}$ is an updated of $(\mathbf{Z}^r)^{-1}\mathbf{u}$. The SMCG is employed at this step to speed up the product $\mathbf{Z}^r\mathbf{v}$.

We choose a neighborhood distance r_d as the distance which defines the boundary between the weak and strong element of the impedance matrix. Then the impedance matrix of rough surface is decomposed into the sum of a strong matrix $\mathbf{Z}^{r,(\text{strong})}$ and a weak matrix $\mathbf{Z}^{r,(\text{weak})}$.

$$\mathbf{Z}^r = \mathbf{Z}^{r,(\text{strong})} + \mathbf{Z}_r^{r,(\text{weak})} \tag{42}$$

where $\mathbf{Z}^{r,(\text{strong})}$ represents near field strong interaction and $\mathbf{Z}^{r,(\text{weak})}$ represents non-near field weak interaction. The strong matrix $\mathbf{Z}^{r,(\text{strong})}$ is a sparse matrix which needs to be stored in the compute process. And the weak matrix $\mathbf{Z}^{r,(\text{weak})}$ is a Toeplitz matrix, so the weak matrix elements can be expanded in a Taylor's series about the horizontal distance between the two points

$$\mathbf{Z}^{r,(w)} = \sum_{m=0}^{M} \mathbf{Z}_m^{r,(\text{weak})} \tag{43}$$

The zeroth term of above equation is called the flat surface contribution.

$$\mathbf{Z}^{r,(FS)} = \mathbf{Z}_0^{r,(\text{weak})} \tag{44}$$

Then the equations are solved using iterative method liking the Pre-BICGtab. The matrix-vector products of $\mathbf{Z}^{r,(FS)}\mathbf{v}$ and $\mathbf{Z}^{r,(\text{weak})}\mathbf{v}$ can be computed quickly by using a 2-D FFT algorithm (as shown in Figure 3), and $\mathbf{Z}^{r,(\text{strong})}\mathbf{v}$ is computed by using traditional MoM method. As a result, the complexity of SMCG is $O(N \log N)$.

As a conclusion, we call E-PILE+SMCG this method, in order to differentiate it from the PILE method for 2D scattering problem. Because the unknown number of rough surface is much larger than that of object, so the complexity of E-PILE+SMCG is approximately the same to that of SMCG.

2.4. The Bistatic Scattering Coefficient and Angular Correlation Function

After the surface currents are solved, the scattered fields in medium 0 can be calculated. The scattering amplitudes for both the co-polarized and cross-polarized polarization s $F_{\beta\alpha}$ are respectively [9, 570–572]

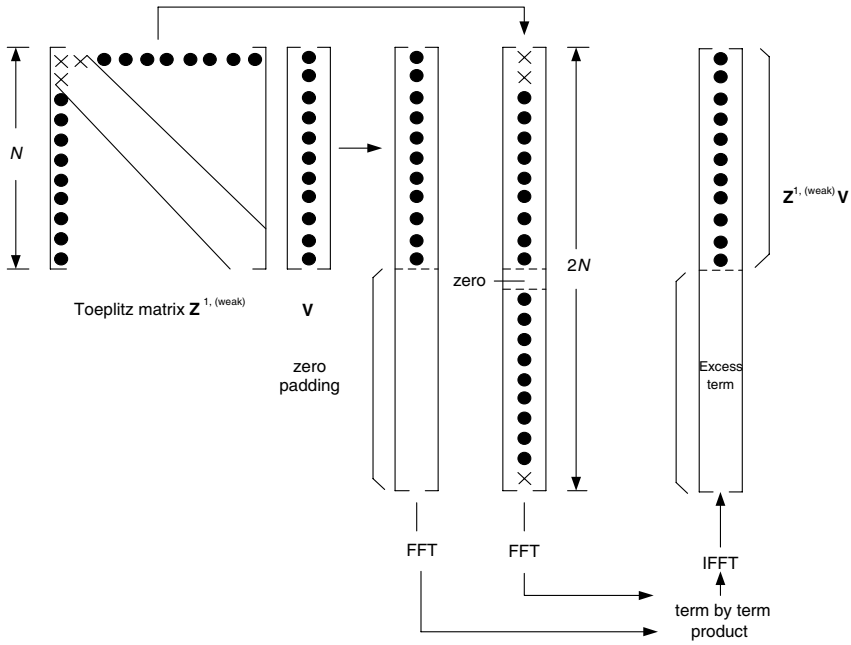

Figure 3. Scheme of the FFT acceleration of the product $\mathbf{Z}^{r,(\mathrm{weak})}\mathbf{v}$ when $\mathbf{Z}^{r,(\mathrm{weak})}$ a Toeplitz matrix.

$$\begin{aligned} F_{h\alpha} &= \frac{ik_0}{4\pi\sqrt{2\eta P_\alpha^i}}\exp(-ikr)\int_S \big[(M_{rx}(\mathbf{r}')\cos\theta_s\cos\phi_s \\ &\quad +M_{ry}(\mathbf{r}')\cos\theta_s\sin\phi_s - M_{rz}(\mathbf{r}')\sin\theta_s) \\ &\quad -\eta(J_{rx}(\mathbf{r}')\sin\phi_s - J_{ry}(\mathbf{r}')\cos\phi_s)\big]\,ds \end{aligned} \tag{45a}$$

$$\begin{aligned} F_{v\alpha} &= \frac{ik_0}{4\pi\sqrt{2\eta P_\alpha^i}}\exp(-ikr)\int_S \big[(M_{rx}(\mathbf{r}')\sin\phi_s \\ &\quad -M_{ry}(\mathbf{r}')\cos\phi_s) + \eta(J_{rx}(\mathbf{r}')\cos\theta_s\cos\phi_s \\ &\quad +J_{ry}(\mathbf{r}')\cos\theta_s\sin\phi_s - J_{rz}(\mathbf{r}')\sin\theta_s)\big]\,ds \end{aligned} \tag{45b}$$

where, h means horizontal polarization, and v means vertical polarization, $\mathbf{M}_r(\mathbf{r}) = M_{rx}\hat{\mathbf{x}}+M_{ry}\hat{\mathbf{y}}+M_{rz}\hat{\mathbf{z}}$, $\mathbf{J}_r(\mathbf{r}) = J_{rx}\hat{\mathbf{x}}+J_{ry}\hat{\mathbf{y}}+J_{rz}\hat{\mathbf{z}}$. The scattering amplitudes in (32) are normalized by the square root

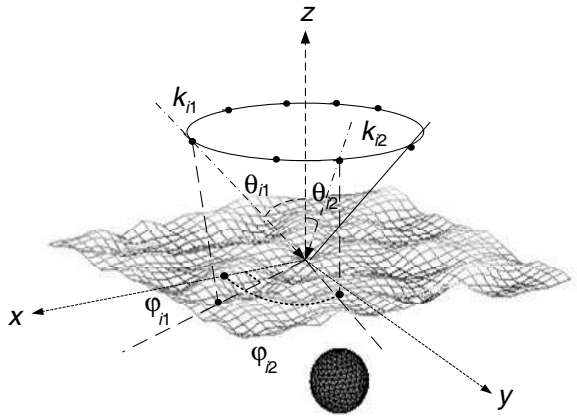

Figure 4. The geometry of azimuthal averaging.

of the incident power $2\eta P_\alpha^{inc}$, which is given as

$$p_\alpha^{inc} = \frac{2\pi^2}{\eta} \int\limits_{k_\rho < k_0} dk_x dk_y |E_{i\alpha}(k_x, k_y)|^2 \frac{k_z}{k_0} \tag{46}$$

Since the buried object is under a single random rough surface, the realization averaging that is usually done in random rough surface scattering simulations is not applicable. In the numerical results, both the bistatic scattering coefficient (BSC) and ACF are calculated based on azimuthal averaging (as shown in Figure 4).

Let N_φ be the number of zaimuthal angles. The bistatic scattering coefficient is

$$\sigma_{\beta\alpha}(\theta_s, \theta_i) = \frac{1}{N_\varphi} \sum_{n=1}^{N_\varphi} |F_{\beta\alpha}(\theta_s, \varphi_{sn}; \theta_i, \varphi_{in})|^2 \tag{47}$$

The ACF is the correlation function of two scattered fields in directions θ_{s1} and θ_{s2}, corresponding to two incident fields in θ_{i1} and θ_{i2}, respectively. The ACF of scattered fields from rough surface exhibits a strong correlation known as the angular memory effect, which is generally small away from the memory line [20, 21]. The memory line obeys the angular relation $\sin\theta_{s2} - \sin\theta_{s1} = \sin\theta_{i2} - \sin\theta_{i1}$, which is a consequence of the statistical translation invariance of the random rough surface. And the ACF can be calculated as following

$$\begin{aligned} &\Gamma_{\beta\alpha}(\theta_{s2}, \theta_{i2}; \theta_{s1}, \theta_{i1}) \\ &= \frac{1}{N_\varphi} \sum_{n=1}^{N_\varphi} F_{\beta\alpha}(\theta_{s2}, \varphi_{s2n}; \theta_{i2}, \varphi_{i2n}) F^*_{\beta\alpha}(\theta_{s1}, \varphi_{s1n}; \theta_{i1}, \varphi_{i1n}) \end{aligned} \tag{48}$$

where φ_{in} and φ_{sn} are incident and scattering azimuthal angles. In the scattering plane, they are related to each by the realizations of $\varphi_{sn} = \varphi_{in}$ for θ_s having the same sign as θ_i, $\varphi_{sn} = \varphi_{in} + 180^\circ$ for θ_s having the opposite sign as θ_i.

3. NUMERICAL RESULTS

The soil's rough surface profiles used in the study are realizations of a rough surface with a Gaussian spectrum

$$W(k_x, k_y) = \frac{l_x l_y h^2}{4\pi} \exp\left(-\frac{l_x^2 k_x^2 + l_y^2 k_y^2}{4}\right) \tag{49}$$

Here, l_x and l_y are the correlation lengths in x- and y-directions, respectively, and h is the rms height of the rough surface.

In order to study the convergence of E-PILE+SMCG versus its order P_{PILE}, define the Relative Error (RE) of nth order as

$$\text{RE: } \tau(n) = \frac{\text{norm}\left|\mathbf{Z}^r\left(\mathbf{X}_r^{(n)} - \mathbf{X}_r^{(n-1)}\right)\right|}{\text{norm}\left|\mathbf{V}^{inc}\right|} \tag{50}$$

The norm of a vector of components X_i and of length N is expressed as norm $(\mathbf{X}) = \sum_{i=1}^{i=N} |X_i|^2$. The vector $\mathbf{X}_r$ represents the current on the rough surface. The vector $\mathbf{V}^{inc}$ represents the initial incident field.

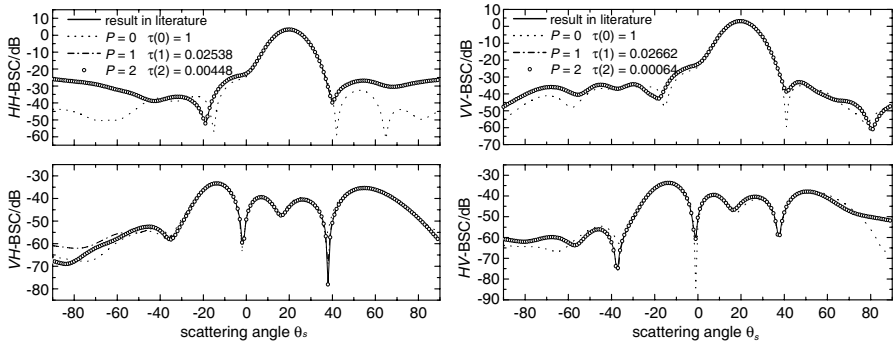

Figure 5. The BSC of a buried sphere.

3.1. Validation and Efficiency of the Method

In Figure 5, the E-PILE+SMCG computer code is compared with the method published in [9, Chapter 11, Volume 2]. The buried object is assumed to be a PEC sphere of radius $r = 0.3\lambda$ at burial depth $d = 0.6\lambda$, where the incident angle is $\theta_i = 20°$, $g = L/4$ (L is L_x or L_y in this case) and the relative dielectric constant of the soil is $\varepsilon_r = 2.0 + 0.2i$. The sphere surface is discretized into 240 triangle patches. The sizes of the rough surface in the x and y directions are $L_x = L_y = 8.0\lambda$. The surface rms height is $h = 0.02\lambda$, and the correlation lengths are $l_x = l_y = 0.5\lambda$. The surface is sampled at 64 points per λ^2 giving 4096 points on the rough surface and 24576 surface unknowns. The bistatic scattering coefficient (BSC) for HH-polarization (HH-BSC) and VH-polarization (VH-BSC) are shown in Figure 5(a). The BSC for VV-polarization (VV-BSC) and HV-polarization (HV-BSC) are shown in Figure 5(b). The RE of every order is also shown in Figure 5. From Figure 5, we can know that the result of E-PILE+SMCG is well agreement with that in [9] when RE is smaller than 10^{-2}, and the largest error between two methods is 0.2 dB. So, in the following examples, the iteration process is terminated when RE is smaller than 10^{-2}. At the same time, the RE decreases when the order P increases, so one can conclude that good convergence is obtained.

3.2. The Comparison between BSC and ACF

We calculate the scattering amplitudes for 10 azimuthal angles at 0°, 36°, 72°, ..., and 324°, respectively. There is only one realization of the random rough surface. The BSC and ACF are calculated

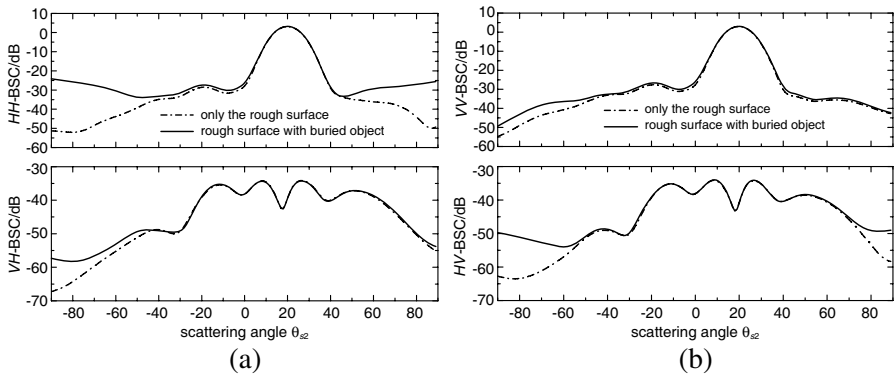

Figure 6. The BSC of a buried sphere.

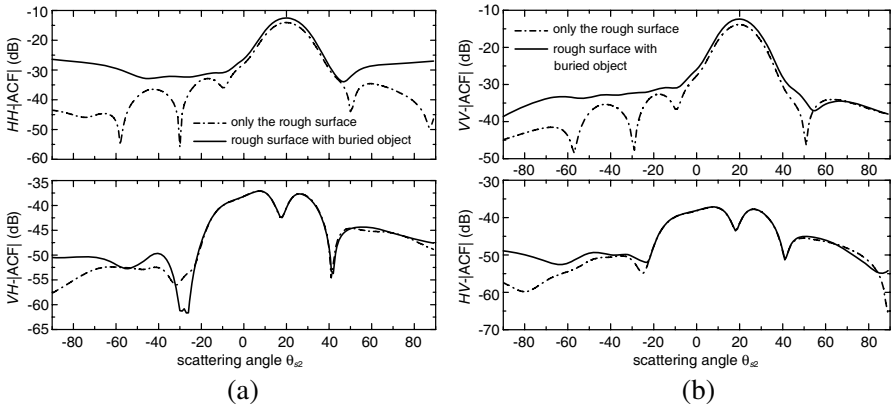

Figure 7. The ACF of a buried sphere.

by using azimuthal angular averaging as given in Equations (47) and (48). The results are plotted as function of the scattering angle θ_{s2}. Parameters for other angles are $\theta_{i1} = 20°$, $\theta_{s1} = -20°$, and $\theta_{i2} = 20°$. The fully polarimetric results of BSC and ACF are calculated and shown in Figures 6 and 7. Figure 6(a) shows the results of BSC for HH-polarization and VH-polarization component, and the results for VV-polarization and HV-polarization component are shown in Figure 6(b). Both the results with and without the object sphere are shown for comparison. As expected, there is a peak in the specular direction, which is due to the slightly rough surface. We see that the differences of BSC between with and without the object for co-polarizations are larger than those for cross-polarizations. This is because the cross-polarization components are mainly due to the rough surface scattering. Because the object is a sphere, it is only a small cross-polarization contribution in BSC. It is also found that there are larger differences for the VV component than for the HH component. Figure 7 shows the absolute value of ACF for rough surface with and without object, in which $\beta\alpha$-|ACF| represents the absolute value of ACF for $\beta\alpha$-polarization. We can see the large difference of |ACF| between with and without an object in both the co-polarization and cross-polarization result. As shown in Figure 7, the difference of |ACF| is large even for angles closed to the nadir direction. This is because the memory effect is avoided and rough surface scattering is minimized in the |ACF|. As a conclusion, the difference of |ACF| for rough surface with and without object is larger than that of BSC, which shows that the ACF has great advantage for detecting buried object over BSC.

3.3. The Relationship between ACF and Rough Surface Profile

Figure 8 shows the amplitude of the |ACF| for sphere buried in soil rough surface of three different correlation lengths for fully polarization. The other parameters are given by $h = 0.02\lambda$, $d = 0.6\lambda$, $r = 0.3\lambda$, $L_x = L_y = 8.0\lambda$ and $\varepsilon_r = 2.0{+}0.2i$. The results show that the amplitude of the |ACF| increases as the correlation length increases, especially at specular direction. In particular, the difference of |ACF| for three correlation lengths is larger for the cross-polarization case. Figure 9 shows the amplitude of the |ACF| for sphere buried in soil rough surface of three different rms heights, with $d = 0.6\lambda$, $r = 0.3\lambda$, $L_x = L_y = 8.0\lambda$, $lx = ly = 0.02\lambda$ and $\varepsilon_r = 2.0 + 0.2i$. We can see that

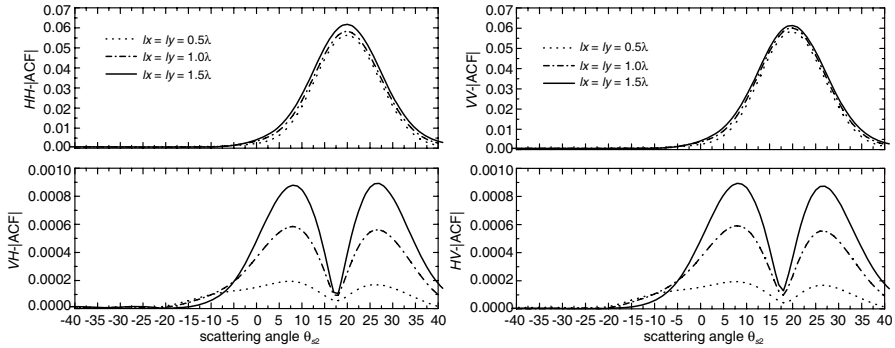

Figure 8. The ACF for different correlation lengths.

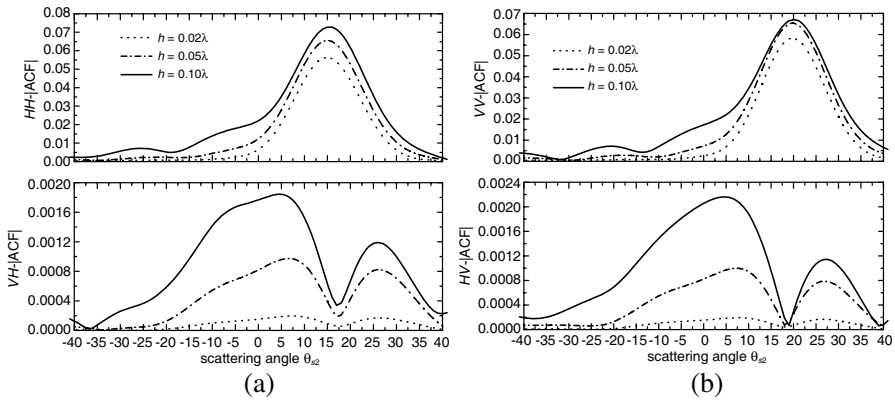

Figure 9. The ACF for different rms heights.

the amplitude of the ACF increases as the rms length increases, not only at specular direction but also at all the other directions, which is different for the case of Figure 8. At the same time, we also found that the difference of the difference of the |ACF| is more distinct for the cross-polarization case because the cross-polarization contribution is directly influenced by roughness of soil surface.

3.4. The Relationship between ACF and Object

Figure 10 shows the amplitude of |ACF| for buried sphere with different depths. The other parameters are $h = 0.02\lambda$, $r = 0.3\lambda$, $lx = ly = 0.5\lambda$, $L_x = L_y = 8.0\lambda$ and $\varepsilon_r = 2.0 + 0.2i$. The results show that the amplitude of the ACF decreases as the depth of the sphere increases because the distance between rough surface profile and object increase as the depth of object increases and because the mutual interaction between buried sphere and the soil rough surface decreases, which finally infects the ACF. The difference of ACF for cross-polarization is small. Figure 11 shows the amplitude of the |ACF| for buried sphere with different radii, with other parameters given by $d = 0.6\lambda$, $h = 0.02\lambda$, $L_x = L_y = 8.0\lambda$, $lx = ly = 0.02\lambda$ and $\varepsilon_r = 2.0 + 0.2i$. As expected, we can see that the amplitude of the ACF increases as the radii of the sphere increases. This is because the mutual interaction between buried object and soil rough surface increases as the radii increases. At the same time, because sphere has small contribution for cross-polarization scattering, the difference of the ACF for cross-polarization is smaller than that for co-polarization.

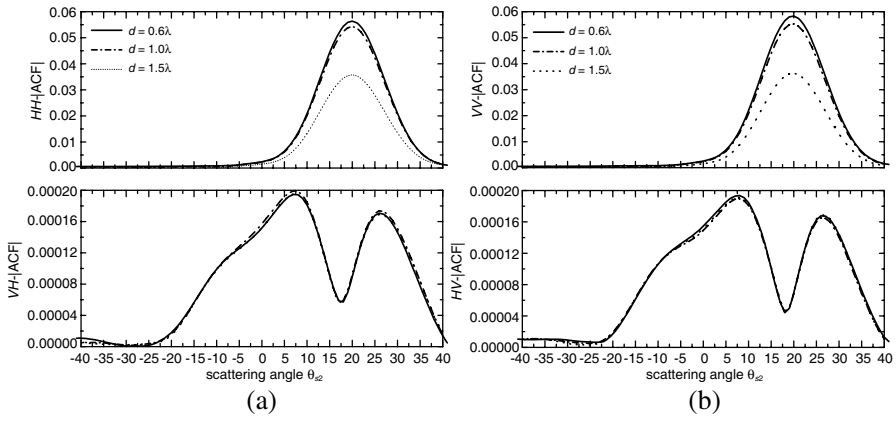

Figure 10. The ACF for buried sphere with different depths.

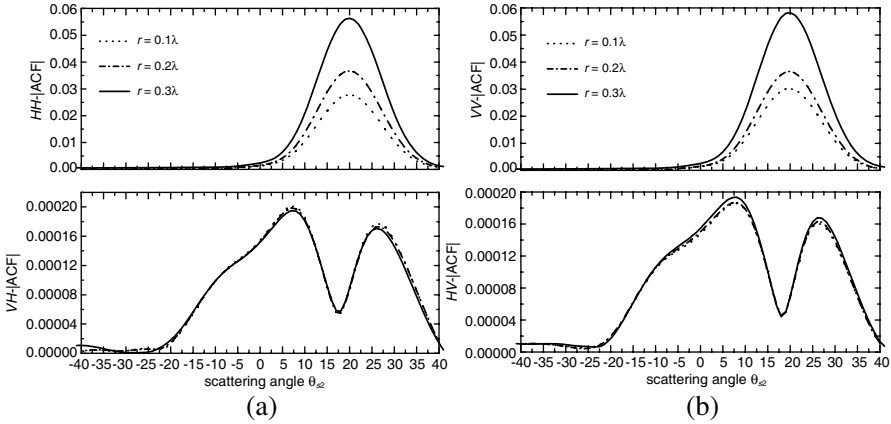

Figure 11. The ACF for buried sphere with different radii.

4. CONCLUSIONS

By extending the PILE method which is introduced for 2D scattering problem, a rigorous fast numerical method E-PILE+SMCG is proposed for scattering from 2D rough surface with 3D buried object (3D problem). The SMCG method is used for accelerating the calculation the integral equations of the rough surface, and the object is computed by traditional MoM. The complexity of this method is similar to that of SMCG ($N \log N$). Then this method is used to compute the scattering from soil rough surface with buried sphere object. In Figure 5, the results of E-PILE+SMCG are in agreement with that in literature, which shows the validity of this method. At the same time, the convergence of E-PILE+SMCG is also discussed. Then, this method is used to study the scattering field and ACF of soil rough surface with buried object. In Figures 6 and 7, the results show that the ACF has great advantage for detecting buried object over BSC. At last, the ACF is studied for different parameters of rough surface such as rms height and correction length and for different parameters of sphere object such as radii and depth. The simulation result shows that the ACF can be influenced greatly by parameters of rough surface and object, and this characteristic can be very useful in realistic detecting technology.

ACKNOWLEDGMENT

This work was supported by the State Key Lab. of Millimeter Waves, Nanjing, China (Grant No. K200907). The authors would like to thank the reviewers for their constructive suggestions.

REFERENCES

1. Zhang, Y., Y. E. Yang, H. Braunisch, and J. A. Kong, "Electromagnetic wave interaction of conducting object with rough surface by hybrid SPM/MOM technique," *Progress In Electromagnetic Research*, Vol. 22, 315–335, 1999.
2. Ishimaru, A., J. D. Rockway, and Y. Kuga, "Rough surface Green's function based on the first-order modified perturbation and smoothed diagram methods," *Waves Random Media*, Vol. 10, 17–31, 2000.
3. O'Neill, K., R. F. Lussky, and K. D. Paulsen, "Scattering from a metallic object embedded near the randomly rough surface of a lossy dielectric," *IEEE Trans. Geosci. Remote Sensing*, Vol. 34, 367–376, 1996.
4. O'Neill, K., "Broadband bistatic coherent and incoherent detection of buried objects beneath randomly rough surfaces," *IEEE Trans. Geosci. Remote Sensing*, Vol. 38, 891–898, 2000.
5. O'Neill, K., "Exploration of innovative radar sensing schemes for subsurface object detection," *Proc. IGARSS'97*, 1135–1137, Singapore, 1997.
6. Dogaru, T. and L. Carin, "Time-domain sensing of targets buried under a rough air-ground interface," *IEEE Trans. Antennas Propagat.*, Vol. 46, 360–372, 1998.
7. Johnson, J. T. and R. J. Burkholder, "A study of scattering from an object below a rough surface," *IEEE Trans. Geosci. Remote Sensing*, Vol. 42, 59–66, 2004.
8. El-Shenawee, M., C. M. Rappaport, E. L. Miller, and M. B. Silevitch, "Three-dimensional subsurface analysis of electromagnetic scattering from penetrable/PEC objects buried under rough surfaces: Use of the steepest descent fast multipole method," *IEEE Trans. Geosci. Remote Sensing*, Vol. 39, 1174–1182, 2001.
9. Tsang, L., J. A. Kong, and K. H. Ding, *Scattering of Electromagnetic Waves: Numerical Simulations*, New York, 2000.
10. Tsang, L., C. H. Chang, and H. Sangani, "A banded matrix iterative approach to monte carlo simulations of scattering of waves by large scale random rough surface problems: TM case," *Electron. Lett.*, Vol. 29, 1666–1667, 1993.
11. Tsang, L., C. H. Chang, H. Sangani, A. Ishimaru, and P. Phu, "A banded matrix iterative approach to monte carlo simulations of large-scale random rough surface scattering: TE case," *Journal of Electromagnetic Waves and Applications*, Vol. 7, No. 9, 1185–

1200, 1993.

12. Torrungrueng, D., H. T. Chou, and J. T. Johnson, "A novel acceleration algorithm for the computation of scattering from two-dimensional large scale perfectly conducting random rough surfaces with the forward backward mehod," *IEEE Trans. Geosci. Remote Sensing*, Vol. 38, 1656–1668, 2000.
13. Jandhyala, V., E. Michielssen, S. Balasubramaniam, and W. C. Chew, "A combined steepest descent fast multipole algorithm for the fast analysis of three-dimensional scattering by rough surfaces," *IEEE Trans. Geosci. Remote Sensing*, Vol. 36, 738–747, 1998.
14. Ji, W.-J. and C.-M. Tong, "Bistatic scattering from two-dimensional dielectric ocean rough surface with a PEC object partially embedded by using the G-SMCG method," *Progress In Electromagnetics Research*, Vol. 105, 119–139, 2010.
15. Déchamps, N., N. De Beaucoudrey, C. Bourlier, and S. Toutain, "Fast numerical method for electromagnetic scattering by rough layered interfaces: Propagation-Inside-Layer expansion method," *J. Opt. Soc. Amer. A*, Vol. 23, 359–369, 2006.
16. Bourlier, C., G. Kubické, and N. Déchamps, "A fast method to compute scattering by a buried object under a randomly rough surface: PILE combined to FB-SA," *J. Opt. Soc. Amer. A*, Vol. 25, 891–902, 2008.
17. Le, C. T. C., Y. Kuga, and A. Ishimaru, "Angular correlation function based on the second-order Kirchhoff approximation and comparison with experiments," *J. Opt. Soc. Amer. A.*, Vol. 13, 1057–1066, 1996.
18. Kuga, Y., C. Lee, A. Eshimaru, and L. Aies-Sengers, "Analytical, experimental and numerical studies of angular memory signatures of waves scattered from one-dimensional rough surfaces," *IEEE Trans. Geosci. Remote Sensing*, Vol. 34, 1300–1307, 1996.
19. Feng, S., C. Kane, P. A. Lee, and A. D. Stone, "Correlations and fluctuations of coherent wave transmission through disordered media," *Phys. Rev. Lett.*, Vol. 61, No. 7, 834–837, 1988.
20. Michel, T. R. and K. A. O'Donnell, "Angular correlation functions of amplitudes scattered from a one-dimensional, perfectly conducting rough surface," *J. Opt. Soc. Amer. A*, Vol. 9, No. 8, 1374–1384, 1992.
21. Zhang, G., L. Tsang, and Y. Kuga, "Studies of angular correlation function of scattering by random rough surfaces with and without a buried object," *IEEE Trans. Geosci. Remote Sensing*, Vol. 35, 444–453, 1997.

22. Zhang, G., L. Tsang, and K. Pak, "Angular correlation function and scattering coefficient of electromagnetic waves scattered by a buried object under a two-dimensional rough surface," *J. Opt. Soc. Amer. A*, 2995–3002, Dec. 1998.
23. Rao, S. M., D. R. Wlton, and A. W. Glisson, "Electromagnetic scattering by surfaces of arbitrary shape," *IEEE Trans. Antennas Propagat.*, Vol. 32, 409–418, 1982.